J Mol Model (2012) 18:4043–4052
DOI 10.1007/s00894-012-1395-2

ORIGINAL PAPER

Structure and energetics of small iron clusters

Keitel Cervantes-Salguero · Jorge M. Seminario

Received: 10 December 2011 / Accepted: 28 February 2012 / Published online: 31 March 2012

Abstract Electronic properties of $Fe_{2\text{-}10}$ clusters and their ions are described by an all-electron ab initio density functional theory computational analysis using the Handy's OPTX exchange and the gradient-corrected correlation functional of Perdew, Burke and Ernzerhof with a triple-zeta valence basis set plus polarization functions. Ground state structures, magnetic moments, dissociation energies, binding energies, IR vibrational spectra, vertical and adiabatic ionization energies, and electron affinities are reported. Two possible states for Fe_2 which are separated by 81.54 meV are described as possible Fe_2, while the septet (ground state) yields an accurate bond distance (error of 0.02 Å); the nonet yields a precise vibrational frequency (error of 10.1 cm^{-1}). Fe_2 binding energy (0.05 eV/atom error) more closely resembles experimental data than any other previously reported computational methods. In addition, the Fe_6 is found to be the most stable cluster within our set being analyzed.

Keywords Ab initio · DFT · Iron cluster · OPBE · TZV

K. Cervantes-Salguero
Centro de Tecnologías de Información y Comunicaciones,
Universidad Nacional de Ingeniería,
Lima, Perú

J. M. Seminario (✉)
Department of Chemical Engineering, Department of Electrical and Computer Engineering, Materials Science and Engineering Program, Texas A&M University,
College Station, TX, USA
e-mail: seminario@tamu.edu

Introduction

Because of its physical properties, iron is one of the most important ferromagnetic materials among the first-row transition metals (TM). Its high magnetic moments as well as its high values of transverse relaxativity make iron and its oxides a suitable ingredient in magnetic nanoparticles (MNPs). High values of transverse relaxativity are caused by an external magnetic field and facilitate the detection of signals by means of the iron transverse relaxation. MNP-based devices are employed in applications such as biosensing using magnetic resonance [1], detecting tuberculosis bacteria [2], and for magnetic enrichment in *in vivo* detection of circulating tumor cells [3].

From a cluster physics viewpoint, it is difficult to perform an accurate study of iron clusters at empirical and ab initio levels [4, 5]; nevertheless, density functional theory (DFT) has been successfully applied and become popular for computation of TM properties in the last decades [6]. The capability of DFT to consider static correlation allows us to find the correct electronic structure among several low lying states [5], thereby leading us to obtain the correct magnetic and structural properties. Thus, the presence of a strong correlation in partially filled *d* orbitals leads to the highest magnetic moments. Previous computational studies for small iron clusters [7–16] have shown a size-dependence and a larger effective magnetic moment per atom over the bulk value of $2.22\mu_B$; this value is approached experimentally for more than 500 atoms [17]. While iron cluster structures resulted in distorted geometries far away from the crystalline bcc bulk structure, these distortions are predicted by the Jahn-Teller effect [18].

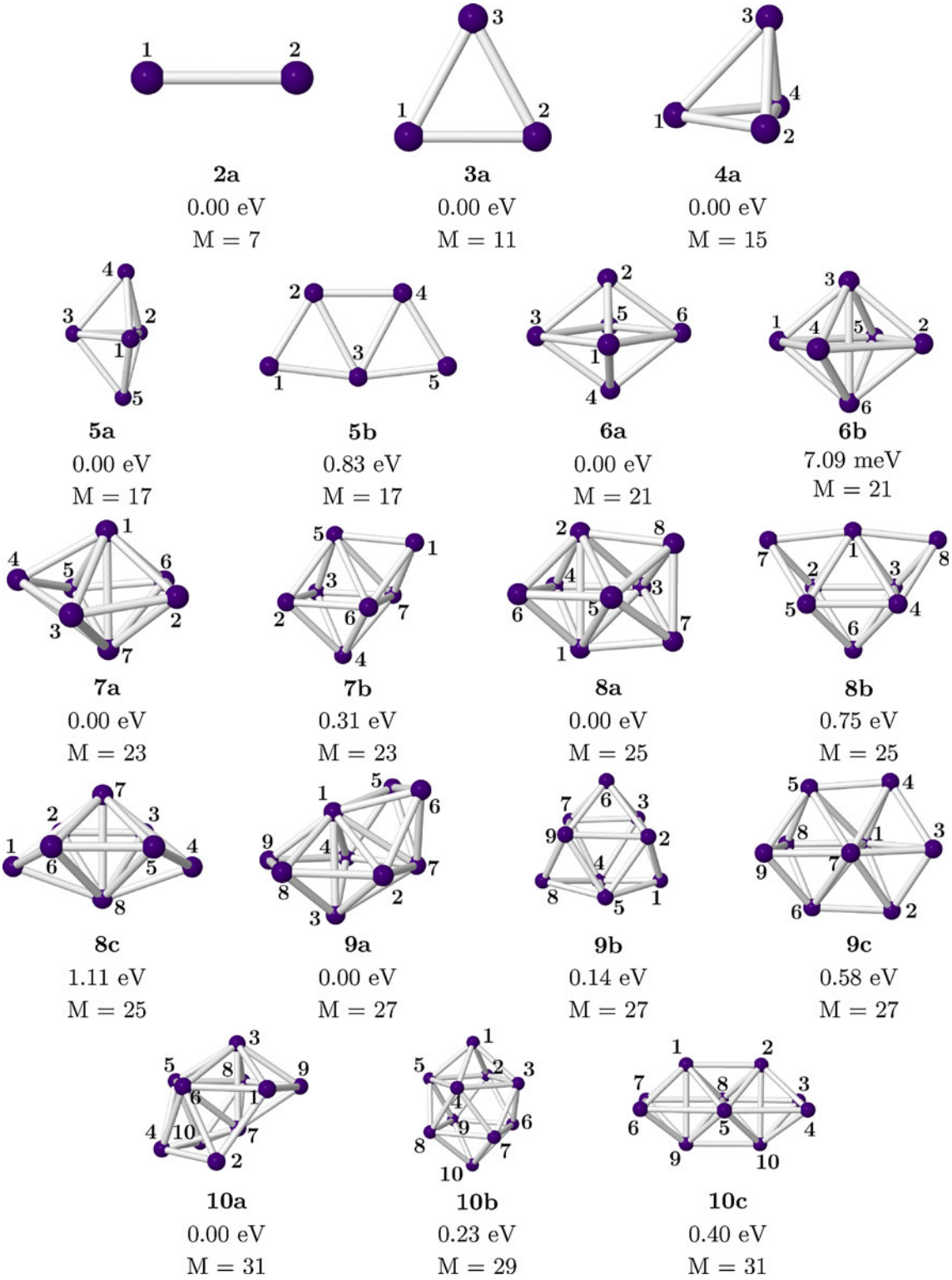

Fig. 1 Optimized structures, relative energies and multiplicities (M) for the Fe_n (n=2-10) lowest conformation found for the ground states (labeled with **a**) and some isomers (labeled **b** with and/or **c**), including an excited state for Fe_{10}

In this work we emphasize the quality of all-electron calculations in the framework of DFT for finding the most stable Fe_n clusters. In addition, we also calculate the iron cluster ions for a deeper understanding of the stability of neutral clusters. Optimized structures are obtained from unconstrained symmetries using the OPBE/TZV level of

Table 1 Optimized distances (d_{mp}) between atoms m and p for the $Fe_{n=2-10}$ ground states shown in Fig. 1

n	d_{12}	d_{23}	d_{34}	d_{45}	d_{56}	d_{67}	d_{78}	d_{89}	$d_{9(10)}$
2	2.003								
3	2.167								
	2.283	2.282							
4	2.239								
	2.566	2.239							
	2.239	2.566	2.239						
5	2.668								
	2.264	2.263							
	2.298	2.299	2.384						
	2.298	2.298	2.382	3.688					
6	2.284								
	2.553	2.285							
	2.284	2.799	2.285						
	3.611	2.284	2.554	2.284					
	2.552	2.283	3.611	2.283	2.553				
7	2.295								
	2.534	2.316							
	2.274	3.656	2.257						
	2.534	3.793	3.678	2.256					
	2.295	2.453	3.793	3.656	2.316				
	2.704	2.331	2.315	2.600	2.315	2.332			
8	2.814								
	2.502	2.501							
	2.239	2.239	2.287						
	2.502	2.501	3.401	3.809					
	2.239	2.239	3.809	2.729	2.286				
	2.278	3.412	2.321	3.792	2.320	3.792			
	3.414	2.278	2.321	3.793	2.321	3.793	2.294		
9	2.424								
	2.632	2.334							
	2.425	3.669	2.334						
	2.311	3.767	3.887	2.355					
	2.312	2.355	3.888	3.768	2.356				
	2.631	2.333	2.481	2.334	2.338	2.338			
	2.312	2.355	2.339	3.768	4.544	3.887	3.887		
	2.311	3.766	2.338	2.355	3.885	4.544	3.886	2.356	
10	2.426								
	2.353	3.896							
	3.868	2.427	3.859						
	3.857	3.895	2.416	2.354					
	2.353	2.316	2.442	2.353	2.441				
	2.363	2.305	2.536	2.363	2.536	2.530			
	3.878	4.645	2.358	3.879	2.359	3.893	2.403		
	2.391	3.966	2.323	4.575	3.860	3.868	2.274	2.419	
	4.575	3.968	3.859	2.392	2.323	3.867	2.273	2.417	3.932

theory. For further reading on the OPBE performance in the prediction of the correct spin states of iron complexes the reader is forwarded to [19]. The next section briefly reviews the methodology, the third section shows the results of our ab initio calculations and the final section discusses the conclusions.

Methods

Calculations are performed in the framework of DFT using the Gaussian-09 program [20]. We choose the OPBE functional, which is a combination of the Handy's OPTX modification of the Becke's exchange functional [21, 22], and the gradient-corrected correlation functional of Perdew, Burke and Ernzerhof of (PBE) [23, 24]. The basis set used is the triple-ζ valence (TZV) basis set also known as {842111/631/411} [25]. Our earlier work using DFT has produced acceptable results when compared to available experimental data [26–45].

All of the structures are initially optimized using quadratic convergence with a threshold of 10^{-6} for the self-consistent field (SCF) wavefunction due to the difficulty to reach convergence with the default settings. The initially optimized structures and wavefunctions are finally used as inputs to optimize them with the default threshold of 10^{-8}.

All of the geometry optimizations are carried out with the Berny algorithm using the geometry-optimization energy-represented direct inversion in the iterative subspace (GEDIIS) algorithm, which is implemented by default in Gaussian-09.

We do not impose any symmetry constraints; however, calculations are restricted to collinear arrangement of magnetic moments. The convergence criteria are the default values in the program, 4.5×10^{-4} a.u. and 1.8×10^{-4} Å for the maximum force and displacement, respectively.

In our spin-polarized calculations, unpaired spin populations are obtained by a Mulliken population analysis. Energies of the optimized structures are reported here, including the zero-point energy (ZPE) correction. The optimized structures are verified as local minima by finding no imaginary frequencies.

In addition, we analyze the stability and electronic properties of iron clusters based on size evolution of the magnetic moment per atom, binding energy per atom, the dissociation energy, the first vertical and adiabatic ionization energy and electronic affinity. The average binding energy per atom is defined as

$$E_b(n) = [E_n - nE_1]/n \tag{1}$$

and the dissociation energy is computed from

$$D_e(n) = (E_{n-1} + E_1) - E_n = (n-1)E_b(n-1) - nE_b(n), \tag{2}$$

where E_n is the total energy of $Fe_{n=2\text{-}10}$ including the ZPE correction.

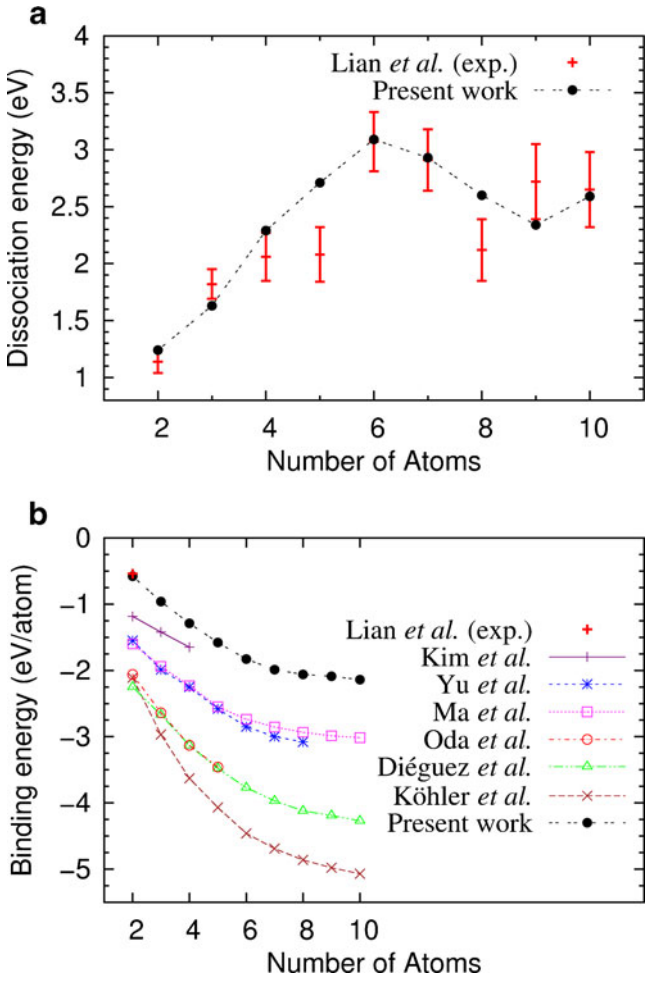

Fig. 2 Fe_n (n=2-10) ground states. Our calculated binding energies are the smallest among other reports. Our calculated dimer value of -0.62 eV/atom is the closest to the experimental value of -0.57 eV/atom

The ionization energy (IE) and electron affinity (EA) are defined as

$$IE = E(Fe_n^+) - E(Fe_n) \tag{3}$$

and

$$EA = E_n(Fe_n) - E(Fe_n^-), \tag{4}$$

respectively. Where $E(Fe_n^+)$, $E(Fe_n^-)$ and $E(Fe_n)$ are the total energies of the cation, anion, and neutral clusters, respectively, all of which are calculated at the optimized geometries of the neutral cluster for the vertical calculations, and at their corresponding relaxed geometries for the adiabatic cases.

Table 2 Bond distance (d_o), frequency (ω_o) and bond dissociation energy (D_e) for the iron dimer

	d_o(Å)		ω_o(cm^{-1})		D_e(eV)	
Experimental	2.02±0.02 [51]		299.6 [66]		1.14 eV±0.10 eV [60]	
Multiplicity (M)	7	9	7	9	7	9
OPBE/TZV	2.00	2.16	397.9	309.5	1.24	1.16

In order to analyze stability, the chemical hardness [46–48] is defined in the framework of DFT as the second derivative of the total energy E_n with respect to the number of electrons, n, at a fixed external potential $v(r)$. According to DFT, it is also the second derivative of the electronic energy with respect to the number of electrons, n, when the external potential, $v(r)$ is kept fixed:

$$\eta = \frac{1}{2}\left(\frac{\partial^2 E_n}{\partial n^2}\right)_{v(r)} = \frac{1}{2}\left(\frac{\partial \mu}{\partial n}\right)_{v(r)} \approx \frac{I-A}{2}, \quad (5)$$

where μ is the chemical potential; I and A are the vertical IE and EA, respectively, from a finite difference approximation; then, using Koopmans's theorem, we can approximate hardness as:

$$\eta \approx \frac{1}{2}(\epsilon_{LUMO} - \epsilon_{HOMO}), \quad (6)$$

where the difference $\epsilon_{LUMO} - \epsilon_{HOMO}$ is the energy gap between the unoccupied and occupied orbitals [49].

Results and discussion

The ground state neutral clusters and their pair distances are shown in Fig. 1 and Table 1, respectively. In general, the optimized geometries and magnetic moments of the ground states are similar to previous reports [10, 11, 13, 16, 50]. The ground states and isomers from the Fe_3 to the Fe_{10} clusters are distorted from the symmetrical forms because of the Jahn-Teller effect. According to the Jahn-Teller theorem, if the highest occupied molecular orbital (HOMO) of a non-linear molecule in a symmetrical conformation is not fully occupied, asymmetrical structural distortions (Jahn-Teller effect) occur to remove the degeneracy.

Energetic and structural analysis of clusters $Fe_{2\text{-}10}$: ground states and isomers

The septet and nonet spin states of the dimer are only separated by 81.54 meV, with the septet as the lowest energy state and yielding the closest bond length of 2.003 Å to the experimental value of 2.02 Å [51]. This is also in good agreement with previous computational studies [7, 52–55] that consider the septet as ground state. However, an experiment performed by Leopold et al. [56, 57] suggested the $^9\Sigma_g^-$ as the ground state. Thus, predicting the dimer as being a septet is not conclusive because both the septet and nonet have similar probabilities to be found in experiments and also because we find the vibrational frequency of the nonet to be the closest to the reported experimental value. These results are summarized in Table 2.

The potential energy surface of the Fe trimer has several local minima [58]; therefore, several optimized structures are possible for the ground state. We find that the Fe_3 ground state is approximately an isosceles triangle of 2.17 Å base and 2.28 Å legs with M=11, in agreement with [11, 52, 59]. While a possible isomer could have a linear geometry with the same multiplicity, other multiplicities with linear geometries show imaginary frequencies.

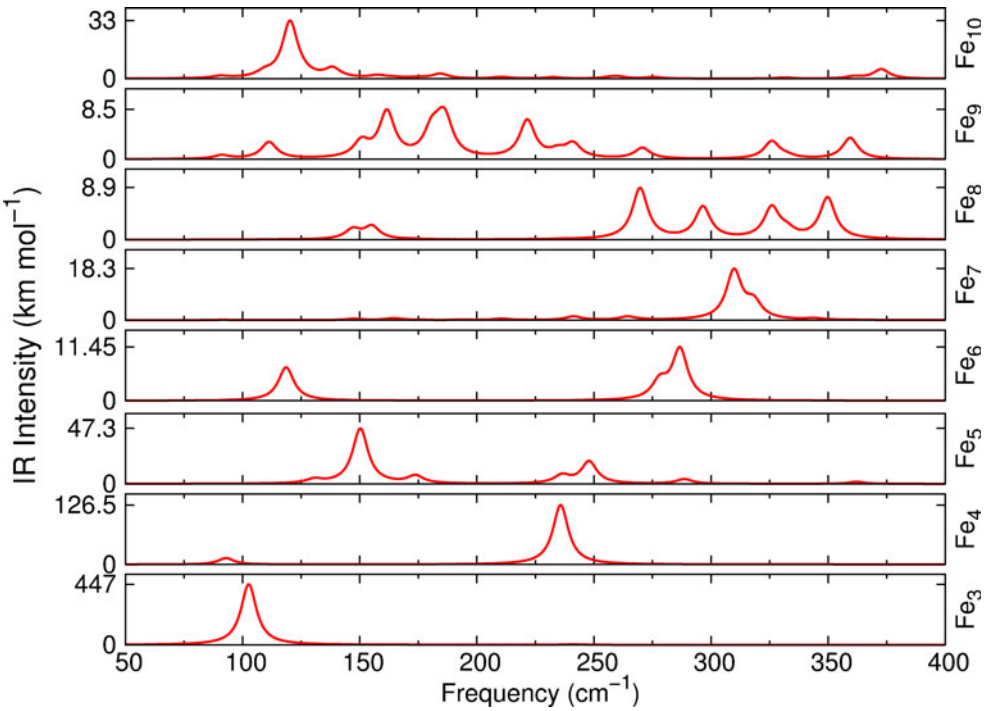

Fig. 3 The infrared spectrum is shown for Fe_n (n=3-10). In the case of Fe_3 we obtained a strong peak at 103 cm^{-1}, and two very small peaks at 241 cm^{-1} and 350 cm^{-1}. Strong peaks indicate antisymmetrical stretching modes

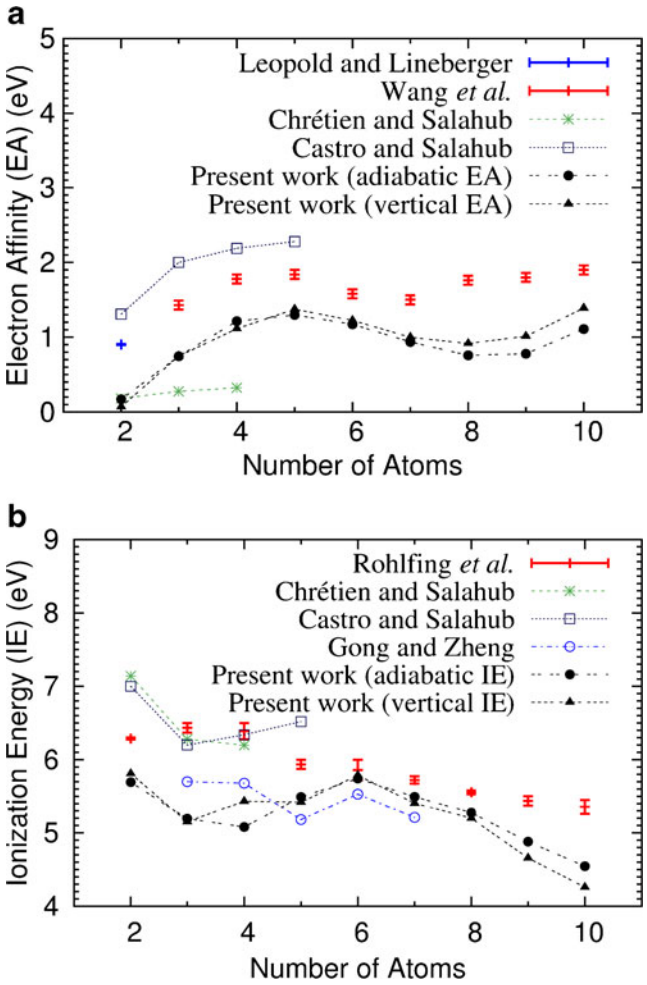

Fig. 4 Ionization energy and electron affinity (adiabatic and vertical) for Fe_n (n=2-10)

The ground state of the tetramer is a distorted tetrahedron **4a** of D_{2d} symmetry with four short 2.24 Å and two long 2.57 Å bond lengths, in excellent agreement with the non-collinear GGA pseudopotential approach reported by Hobbs et al. [14].

Our calculations find a distorted trigonal bipyramid **5a** as the ground state, with minimum bond length of 2.26 Å. A second isomer is the C_{2v} planar structure **5b**. The Fe_5 isomers are stable with $3.2\mu_B$/atom.

Despite the increased number of isomers, the octahedron is found to be the ground state of the hexamer. There are two predicted octahedral forms (**6a** and **6b**) which are separated by 7.09 meV. **6a** has a square base of side 2.55 Å and the separation between the top and bottom atoms is 2.8 Å. The second isomer **6b** has a rectangle base of sides 2.72 Å and 2.31 Å, whose maximum inter-atomic distance is 2.95 Å. All the hexamer structures have the same multiplicity of 21.

A distorted pentagonal bipyramid-like structure **7a** is the ground state, followed by the capped octahedron (C_{3v}) isomer **7b**. Their energy difference is about 0.31 eV. However, results from Ma et al. [11] and Yu et al. [50] showed a regular pentagonal bipyramid (D_{5h}) 21.48 meV and 1.13 eV below the C_{3v} structure, respectively.

For the Fe_8 cluster, the bidisphenoid structure (D_{2d}) is the lowest in energy with a magnetic moment of $3\mu_B$/atom. A structure with similar energy (0.75 eV) is the bicapped octahedron **8b**, which is in the same isomer order as in Yu et al. [50] (0.59 eV). The capped pentagonal bipyramid converge without symmetry constraints to our ground state **8a**. Another isomer structure (D_2) is found at 1.29 meV higher in total energy by Ma et al. [11]; however, the D_2 geometry showed a convergence to our bidisphenoid structure. Our third isomer is characterized by a distorted hexagonal bipyramid **8c**.

The first three Fe_9 isomers are in good agreement with Ma et al. [11]. However, the order for the first two isomers (a regular bicapped pentagonal bipyramid **9a** and an irregular tricapped trigonal prism structure **9b**) were not the same as shown for the first two isomers in Kohler et al. [10] and Diéguez et al. [13]. Also, Rollmann et al. [12] found our third isomer **9c** as their ground state.

The Fe_{10} lowest energy structure **10a** is a C_{3v} symmetry group of multiplicity 31; however, this structure was referred [10, 13] to as the second isomer with M=29. A D_{4d} structure **10b** with a multiplicity of 29 is predicted as the second isomer; to some extent, Ma et al. [11] found such a structure as the ground state, but with M=31. A D_{2h} geometry **10c** with M=31 is predicted as the third isomer.

Table 3 Total energy including ZPE (E_n), HOMO-LUMO gap for alpha and beta electrons (HLG_α and HLG_β), vertical ionization energy (IE), electron affinity (EA) and chemical hardness (η) for the Fe_n clusters

n	E_n (Ha)	HLG_α (eV)	HLG_β (eV)	IE (eV)	EA (eV)	η (eV)
2	-2527.85780	1.22	**0.36**	5.81	0.07	2.87
3	-3791.82392	**0.22**	0.54	5.15	0.75	2.20
4	-5055,81431	**0.58**	0.60	5.43	1.11	2.16
5	-6319,82017	**0.39**	0.55	5.42	1.38	2.02
6	-7583.83977	2.00	**0.52**	5.79	1.22	2.28
7	-8847.85368	1.76	**0.39**	5.41	1.00	2.20
8	-10111,85532	1.92	**0.54**	5.20	0.92	2.14
9	-11375.84750	1.28	**0.51**	4.66	1.01	1.82
10	-12639,84878	**0.15**	0.51	4.26	1.39	1.44

Dissociation energy and binding energy analysis of clusters Fe_{2-10}

In the case of the iron dimer dissociation energy, the error is 0.1 eV comparing the present computational value of 1.24 eV and the experimental value of 1.14±0.10 eV [60] (-0.57 eV/atom for the binding energy, $E_b(n=2)=-D_e(n=2)/2$). In general, the dissociation energy (Fig. 2a) follows a growing behavior up to the Fe_6 cluster, meaning it is the most stable structure in our domain of analysis. The Fe_3 dissociation energy necessary to form Fe_2 and Fe is 1.63 eV in contrast with the experimental value of 1.82±0.13 eV [60]. The maximum error of 0.63 eV (Fe_5) and the overestimated values can be explained because of the mixture of electronic states in the iron clusters, as well as geometries, in the experiment. Figure 2a only considered the ground states and not the isomers. The dissociation energy of the planar **5b** is about 1.89 eV in contrast with the experimental value of 2.08±0.24 eV. The Fe_8 isomers are 1.85 eV (**8b**) and 1.49 eV (**8c**) in contrast with the experimental value of 2.12±0.27 eV. This suggests the important role of multiplicities and geometries in the experiment, i.e. the experimental dissociation energy is an average of the isomers. This explanation fails for both Fe_3 and Fe_9.

The decay behavior of the binding energy curve (Fig. 2b) means that the neutral structures are stable. These values are in favor of being the smallest among other computational methods: LDA+U [61], DFTB [10], BPW91/LANL2DZ [50], BLYP/DNP [11], LSDA [12] and non collinear LSDA [9].

Spectroscopy analysis of clusters Fe_{2-10}

The IR vibrational spectra of the ground states are shown in Fig. 3. For the Fe_3, we obtain a strong peak (antisymmetric mode) at 102.6 cm^{-1} and two weak peaks (symmetrical mode) at 241 cm^{-1} and 350 cm^{-1}. The assignment of the symmetrical stretching mode at 241 cm^{-1} is given by considering the vibrational frequency of the Fe_2 nonet state (309.5 cm^{-1}). This mode also corresponds with the one found by Haslett et al. at 249 cm^{-1}. Moreover the mode at 102.6 cm^{-1} corresponds with the antisymmetric stretching mode at 180 cm^{-1} found by Nour et al. [62].

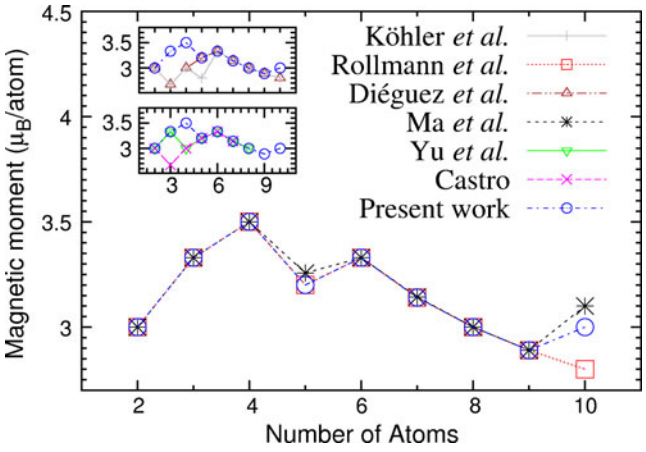

Fig. 5 Size evolution of the magnetic moment (μ_B/atom) for our Fe_n (n=2-10) ground states compared with previous computational methods

Ionization potential, electro affinity, and HOMO-LUMO relations

We calculate adiabatic and vertical IE and EA for the Fe_{2-10} ground states. Adiabatic energies are obtained by the optimization of several structures and multiplicities, whereas for the vertical transitions calculations both energies are computed at the equilibrium geometries of the neutral clusters. ZPE corrections are taken into account for both vertical and adiabatic values. Figure 4 summarizes IE and EA results, where other high level theoretical [52, 55, 63] and experimental data [56, 64, 65] are shown. We show the adiabatic non-local results from Castro and Salahub [55] and the adiabatic results from Chrétien and Salahub [52]. Vertical values are from Gong and Zheng [63].

All vertical and adiabatic multiplicities (for anion and cation) are the same except for those of Fe_6 that have multiplicities of 20 and 22 for the vertical and adiabatic cationic cluster, respectively. Moreover, all the relaxed ionic forms tend to have a similar like-structure as the isomer they originate from, except for the Fe_6 which in both adiabatic anionic and cationic prefers the **6b**-like structure. Considering the ZPE correction, the IE and EA values have increased and decreased, respectively, by values less than 0.31 eV in the Fe_{10} case.

Both adiabatic and vertical values are underestimated compared with experimental data. In general, the error is no larger than 1.02 eV in the case of EA and 1.10 eV in IE, except for the adiabatic and vertical Fe_3^+, adiabatic Fe_4^+ and vertical Fe_{10}^+ where the error is with errors less than 1.31 eV compared to the experiment [64]. The most accurate result is for the Fe_6 anion

Table 4 Magnetic moments for the adiabatic ions (μ_B/atom)

n	Cation (μ_B/atom)	Neutral (μ_B/atom)	Anion (μ_B/atom)
2	3.50	3.00	3.50
3	3.00	3.33	3.67
4	2.75	3.50	3.75
5	3.00	3.20	3.40
6	3.50	3.33	3.17
7	3.29	3.14	3.00
8	3.13	3.00	2.88
9	3.00	2.89	3.00
10	2.90	3.00	3.10

and cation, with errors less than 0.41 eV. In addition, the IE and EA of the adiabatic Fe_6 and Fe_5 are the highest (Fe_6 is second in the vertical IE case, after the dimer) in the whole range of analysis, indicating that the hexamer needs more energy to remove one electron and that the pentamer is more stable by releasing energy when adding one electron.

As suggested by the chemical hardness in Table 3, the iron dimer (η) is the most stable theoretically, followed by the hexamer. Adding a third atom to the dimer, increases the interatomic distances (Table 2) and reduces the bond strength and dissociation energy (Fig. 2a). This trend continues up to Fe_6, which shows a high value of η, predicting high stability. Local maxima values of η are found in Fe_6, Fe_7 and Fe_3, which are the second, third and fourth most stable clusters, respectively. However, the HLG shows a different stability order (tetramer, octamer, hexamer). Roy et al. [16] found the octamer, followed by the hexamer and tetramer, as the most stable structure from the HLG analysis.

Magnetic moment and adiabatic ionic magnetic moments of $Fe_{2\text{-}10}$ clusters

The results for the magnetic moment per atom of the neutral clusters are compared with other theoretical calculations in Fig. 5.

For the Fe_4 cluster, the magnetic moment per atom yields its maximum of $3.5\mu_B$ which is the same as the one found with a GGA ultrasoft pseudopotential procedure performed by Šljivančanin et al. [8]. In the case of Fe_6, a 3.33 μ_B/atom is found in agreement with other DFT based calculations: GGA [7, 8, 11, 12, 14, 50], LDA [13, 15] and DFTB [10] studies. All the Fe_9 isomers have a total magnetic moment of 26 μ_B. In the case of the Fe_{10} isomers, all the structures but **10b** (28 μ_B) have a magnetic moment of 30 μ_B.

Table 4 shows the adiabatic ionic magnetic moments. The common pattern is the convergence of the ion magnetic moments to the neutral values, where the highest magnetic moments are from the Fe_3^- and Fe_4^- clusters. Among cations only, Fe_2^+ and Fe_6^+ have the highest magnetic moment per atom, indicating a great number of unpaired electrons, in spite of the fact that the adiabatic cation shows the highest IE. The low total magnetic moment of $11\mu_B$ for Fe_4^+ [7] and its regular tetrahedral structure are corroborated in the present work.

Conclusions

An acceptable performance of the all-electron OPBE/TZV model for searching ground states and their low-lying isomers is obtained for small iron clusters up to ten atoms. Geometrical structures of the neutral clusters are in good agreement with previous computational studies, but a different order in the isomers is obtained for Fe_8, Fe_9 and Fe_{10}. This could be because, for a ground state cluster, some geometries are more energetically favored by different levels of theory. Distortions are in agreement with the Jahn-Teller effect.

Furthermore, multiplicities are accurately predicted, yielding magnetic moments around 3 μ_B. In the case of the Fe_2, two closest low lying spin states are found: the septet and the nonet. Both states are predicted to have a similar probability to be formed; however, the nonet is the state that has the correct vibrational frequency of 299.6 cm^{-1}. This result in the dimer is also supported by the direction that the dissociation energy curve follows.

Our reported binding energy of the dimer is the closest to the only experimental value available; and all the cluster energies are the smallest among those from other level of theoretical studies. Furthermore, the decay behavior of the binding energy curve suggests that our reported cluster structures are the ground states.

Compared with the experimental data, all our IE and EA results are underestimated. The Fe_6 cluster corresponds to the most stable structure in the hardness analysis and shows the highest IE in the range from three to ten iron atoms. Furthermore, the dissociation energy is the highest indicating the most energetically stable cluster.

Acknowledgments KC-S acknowledges all the constant and wiser support given by Carlos Medina, Huber Nieto-Chaupis, José Oliden, Cinthia Capcha and Jacinto Colán (Centro de Tecnologías de Información y Comunicaciones) at the Universidad Nacional de Ingeniería, Lima-Perú and Luis Jauregui (Purdue University). We acknowledge the help from Christian LeBeau and Akash Pernankil (Texas A&M University) for a thorough check of the English as well as the discussions with Karim Salazar and Norma Rangel (Texas A&M University). JMS acknowledges support from the U.S. Defense Threat Reduction Agency (DTRA) through the U. S. Army Research Office (ARO) under grant number W911NF-06-1-0231, the ARO under a Defense University Research Instrumentation Program (DURIP) project number # W91NF-07-1-0199 and under a Multidisciplinary University Research Initiative (MURI) Project # W911NF-11-1-0024.

References

1. Haun JB, Yoon T-J, Lee H, Weissleder R (2010) Magnetic nanoparticle biosensors. WIREs: Nanomed Nanobiotech 2(3):291-304
2. Lee H, Yoon T-J, Weissleder R (2009) Ultrasensitive detection of bacteria using core-shell nanoparticles and an NMR-filter system13. Angew Chem Int Ed 48(31):5657–5660
3. Galanzha EI, Shashkov EV, Kelly T, Kim J-W, Yang L, Zharov VP (2009) In vivo magnetic enrichment and multiplex photoacoustic detection of circulating tumour cells. Nat Nano 4 (12):855-860. http://www.nature.com/nnano/journal/v4/n12/suppinfo/nnano.2009.333_S1.html
4. Morse MD (1986) Clusters of transition-metal atoms. Chem Rev 86(6):1049–1109. doi:10.1021/cr00076a005
5. Harvey JN (2004) DFT computation of relative spin-state energetics of transition metal compounds. Struct Bond 112:151-184

6. Cramer CJ, Thrular DG (2009) Density functional theory for transition metals and transition metal chemistry. Phys Chem Chem Phys 11:10757–10816
7. Castro M (1997) The role of the Jahn-Teller distortions on the structural, binding, and magnetic properties of small Fe_n clusters, n≤7. International J Quantum Chem 64(2):223–230
8. Šljivančanin Ž, Pasquarello A (2003) Supported Fe nanoclusters: evolution of magnetic properties with cluster size. Phys Rev Lett 90 (24):247202 (247204 pp)
9. Oda T, Pasquarello A, Car R (1998) Fully unconstrained approach to noncollinear magnetism: application to small Fe clusters. Phys Rev Lett 80(16):3622–2625
10. Köhler C, Seifert G, Frauenheim T (2005) Density functional based calculations for Fe_n (n≤32). Chem Phys 309(1):23–31. doi:10.1016/j.chemphys.2004.03.034
11. Ma Q-M, Xie Z, Wang J, Liu Y, Li Y-C (2007) Structures, binding energies and magnetic moments of small iron clusters: A study based on all-electron DFT. Solid State Commun 142(1–2):114–119. doi:10.1016/j.ssc.2006.12.023
12. Rollmann G, Entel P, Sahoo S (2006) Competing structural and magnetic effects in small iron clusters. Comput Mater Sci 35 (3):275–278. doi:10.1016/j.commatsci.2004.09.059
13. Diéguez O, Alemany MMG, Rey C, Ordejón P, Gallego LJ (2001) Density-functional calculations of the structures, binding energies, and magnetic moments of Fe clusters with 2 to 17 atoms. Phys Rev B 63 (20):205407 (205406 pp)
14. Hobbs D, Kresse G, Hafner J (2000) Fully unconstrained noncollinear magnetism within the projector augmented-wave method. Phys Rev B 62(17):11556–11570
15. Ballone P, Jones RO (1995) Structure and spin in small iron clusters. Chem Phys Letters 233(5–6):632–638. doi:10.1016/0009-2614(94)01491-d
16. Roy DR, Robles R, Khanna SN (2010) Magnetic moment and local moment alignment in anionic and/or oxidized Fe_n clusters. J Chem Phys 132(19):194305–194307. doi:10.1063/1.3425879
17. Billas IML, Chatelain A, de Heer WA (1994) Magnetism from the atom to the bulk in iron, cobalt, and nickel clusters. Science 265 (5179):1682–1684. doi:10.1126/science.265.5179.1682
18. Ham FS (2000) The Jahn-Teller effect: a retrospective view. J Luminescence 85(4):193–197. doi:10.1016/s0022-2313(99)00187-8
19. Swart M, Ehlers AW, Lammertsma K (2004) Performance of the OPBE exchange-correlation functional. Mol Phys 102(23):2467–2474
20. Frisch MJ et al (2009) Gaussian 09. Gaussian 09 edn, Wallingford, CT
21. Handy NC, Cohen AJ (2001) Left-right correlation energy. Mol Phys 99(5):403–412
22. Hoe WM, Cohen AJ, Handy NC (2001) Assessment of a new local exchange functional OPTX. Chem Phys Lett 341(3–4):319–328. doi:10.1016/s0009-2614(01)00581-4
23. Perdew JP, Burke K, Ernzerhof M (1996) Generalized gradient approximation made simple. Phys Rev Lett 77(18):3865–3868
24. Perdew JP, Burke K, Ernzerhof M (1996) Errata: generalized gradient approximation made simple. Phys Rev Lett 78:1396
25. Schafer A, Huber C, Ahlrichs R (1994) Fully optimized contracted Gaussian basis sets of triple zeta valence quality for atoms Li to Kr. J Chem Phys 100(8):5829–5835. doi:10.1063/1.467146
26. Yan L, Seminario JM (2005) Electronic structure and electron transport characteristics of a cobalt complex. J Phys Chem A 109 (30):6628–6633
27. Balbuena PB, Calvo SR, Lamas EJ, Salazar PF, Seminario JM (2006) Adsorption and dissociation of H_2O_2 on Pt and Pt-alloy clusters and surfaces. J Phys Chem B 110:17452–17459
28. Saenz LR, Balbuena PB, Seminario JM (2006) Platinum testbeds: interaction with oxygen. J Phys Chem A 110(43):11968–11974
29. Yan L, Balbuena PB, Seminario JM (2006) Perfluorobutane sulfonic acid hydration and interactions with O_2 adsorbed on Pt_3 perflurobutane sulfonic acid hydration. J Phys Chem A 110:4574–4581
30. Zhao P, Woolard DL, Seminario JM, Trew R (2006) Mixed-valence transition metal complex based integral architecture for molecular computing (I): attachment of linker molecule to silicon (100)-2x1 surface. Int J High Speed Electronics Syst 16(2):705–712
31. Miao L, Seminario JM (2007) Electronic and structural properties of oligo phenylene ethynylenes on Au(111) surfaces. J Chem Phys 126:184706 (184701-184707)
32. Sotelo JC, Seminario JM (2007) Biatomic substrates for bulk-molecule interfaces: the PtCo-oxygen interface. J Chem Phys 127 (24):244706 (244713 pp)
33. Yan L, Seminario JM (2007) Electron Transport in Nano-Gold–Silicon Interfaces. Int J Quantum Chem 107(2):440–450
34. Hong S, Jauregui LA, Rangel NL, Cao H, Day S, Norton ML, Sinitskii AS, Jorge M. Seminario (2008) Impedance measurements on a DNA junction. J Chem Phys 128:201103 (201101-201104)
35. Salazar PF, Seminario JM (2008) Identifying Receptor-Ligand Interactions through an ab Initio Approach". J Phys Chem B 112 (4):1290–1292
36. Sotelo JC, Seminario JM (2008) Local reactivity of O_2 to Pt_3 on Co_3Pt and related backgrounds. J Chem Phys 128 (20):204701 (204701-204711)
37. Balbuena PB, Wang Y, Lamas EJ, Calvo SR, Agapito LA, Seminario JM (2009) Reactivity of bimetallic nanoclusters toward the oxygen reduction in acid medium. In: Device and materials modeling in PEM fuel cells; topics in applied physics, vol 113. Springer, Berlin, pp 509-532
38. Bellido EP, Bobadilla AD, Seminario JM (2009) Nitroreductasa functionalized zinc oxide nanorod for phonon-enhanced sensing of trinitrotolueno In: Nanoelectronic Devices for Defense and Security Conference. Bahia Mar Beach Resort, Fort Lauderdale
39. Rangel NL, Seminario JM (2009) Single Molecule Transductors, Slope Detectors and Rectifiers Using Graphene Electrodes. In: Nanoelectronic Devices for Defense and Security Conference, Bahia Mar Beach Resort, Fort Lauderdale, Florida
40. Salazar-Salinas K, Jauregui LA, Kubli-Garfias C, Seminario JM (2009) Molecular biosensor based on a coordinated iron complex. J Chem Phys 130:105101 (105101-105109)
41. Sotelo JC, Seminario JM (2009) Protonation of O_2 adsorbed on a Pt_3 island supported on transition metal surfaces. J Chem Phys 131:044709 (044701-044711)
42. Fu ML, Rangel NL, Adams RD, Seminario JM (2010) Synthesis, crystal structure, photophysical properties, and DFT calculations of a bis(tetrathia-calix[4]arene) tetracadmium complex. J Clust Sci 21:867–878
43. Sotelo JC, Seminario JM (2010) Some recent studies on the local reactivity of O_2 on Pt_3 nanoislands supported on mono- and bi-metallic backgrounds. In: Balbuena PB, Subramanian VR (eds) Theory and experiment in electrocatalysis modern aspects of electrochemistry, vol 50. Springer, New York, pp 203–242
44. Cárdenas-Jirón GI, Leon-Plata P, Cortes-Arriagada D, Seminario JM (2011) Electrical characteristics of cobalt phthalocyanine complexes adsorbed on graphene. J Phys Chem C 115(32):16052–16062
45. Fu M-L, Adams RD, Cristancho D, Leon P, Seminario JM (2011) Spectroscopic and photophysical studies of charge-transfer in a Cd_8 thiolate cluster containing a coodinated N-Methyl-4,4-bipyridinium ligand. Eur J Inorg Chem 2011(5):660–665
46. Parr RG, Donnelly RA, Levy M, Palke WE (1978) Electronegativity: the density functional viewpoint. J Chem Phys 68(8):3801–3807

47. Parr RG, Pearson RG (1983) Absolute hardness: companion parameter to absolute electronegativity. J Am Chem Soc 105:7512–7516
48. Perdew JP, Parr RG, Levy M, Balduz JL Jr (1982) Density-functional theory for fractional particle number: derivative discontinuities of the energy. Phys Rev Lett 49(23):1691–1694
49. Seminario JM, Politzer P (eds) (1995) Modern density functional theory: a tool for chemistry. Theoretical and computational chemistry. Elsevier, Amsterdam
50. Yu S, Chen S, Zhang W, Yu L, Yin Y (2007) Theoretical study of electronic structures and magnetic properties in iron clusters (n≤8). Chem Phys Lett 446(1–3):217–222. doi:10.1016/j.cplett.2007.08.035
51. Purdum H, Montano PA, Shenoy GK, Morrison T (1982) Extended-x-ray-absorption-fine-structure study of small Fe molecules isolated in solid neon. Phys Rev B 25(7):4412–4417
52. Chrétien S, Salahub DR (2002) Kohn-Sham density-functional study of low-lying states of the iron clusters $Fe_n^+/Fe_n/Fe_n^-$ (n=1−4). Phys Rev B 66 (15):155425 (155401-155412)
53. Gutsev GL, Bauschlicher CW (2003) Electron affinities, ionization energies, and fragmentation energies of Fe_n clusters (n=2−6): a density functional theory study. J Phys Chem A 107(36):7013–7023. doi:10.1021/jp030288p
54. Gutsev GL, Bauschlicher CW (2003) Chemical bonding, electron affinity, and ionization energies of the homonuclear 3 d metal dimers. J Phys Chem A 107(23):4755–4767. doi:10.1021/jp030146v
55. Castro M, Salahub DR (1994) Density-functional calculations for small iron clusters: Fe_n, Fe_n^+, and Fe_n^- for n≤5. Phys Rev B 49 (17):11842–11852
56. Leopold DG, Lineberger WC (1986) A study of the low-lying electronic states of Fe_2 and Co_2 by negative ion photoelectron spectroscopy. J Chem Phys 85(1):51–55. doi:10.1063/1.451630
57. Leopold DG, Almlof J, Lineberger WC, Taylor PR (1988) A simple interpretation of the Fe_2^- photoelectron spectrum. J Chem Phys 88(6):3780–3783. doi:10.1063/1.453876
58. Rollmann G, Sahoo S, Entel P (2006) Structure and magnetism in iron clusters. In: Sahoo SN, Choudhury PK, Jena P (eds) Nanoscale materials: from science to technology. Nova Science, New York, p 117
59. Gutsev GL, Khanna SN, Jena P (2000) Unambiguous assignment of the ground state of a nearly degenerate cluster. Phys Rev B 62 (3):1604–1606
60. Lian L, Su CX, Armentrout PB (1992) Collision-induced dissociation of Fe_n^+ (n=2−19) with Xe: bond energies, geometric structures, and dissociation pathways. J Chem Phys 97(6):4072–4083. doi:10.1063/1.463912
61. Kim G, Park Y, Han MJ, Yu J, Heo C, Lee YH (2009) Structure and magnetism of small Gd and Fe nanoclusters: calculations. Solid State Commun 149(45–46):2058–2060. doi:10.1016/j.ssc.2009.08.022
62. Nour EM, Alfaro-Franco C, Gingerich KA, Laane J (1987) Spectroscopic studies of nickel and iron clusters at 12 K. J Chem Phys 86(9):4779–4782. doi:10.1063/1.452699
63. Gong XG, Zheng QQ (1995) Local spin-density electronic structures and magnetic properties of small iron clusters. J Phys Condensed Matter 7(12):2421–2428
64. Rohlfing EA, Cox DM, Kaldor A, Johnson KH (1984) Photoionization spectra and electronic structure of small iron clusters. J Chem Phys 81(9):3846–3851. doi:10.1063/1.448168
65. Wang LS, Li X, Zhang HF (2000) Probing the electronic structure of iron clusters using photoelectron spectroscopy. Chem Phys 262 (1):53–63. doi:10.1016/s0301-0104(00)00351-7
66. Moskovits M, DiLella DP (1980) Di-iron and nickeliron. J Chem Phys 73(10):4917–4924. doi:10.1063/1.440021